

SRCN3D: Sparse R-CNN 3D Surround-View Camera Object Detection and Tracking for Autonomous Driving

Yining Shi¹, Jingyan Shen², Yifan Sun², Yunlong Wang¹, Jiaxin Li³, Shiqi Sun⁴, Kun Jiang^{1*}, Diange Yang^{1*}

¹ State Key Laboratory of Automotive Safety and Energy, School of Vehicle and Mobility

² School of Economics and Management ³ School of Software ⁴ Department of Electronic Engineering

Tsinghua University, Beijing, 100084, China

{syn21,shen-jy21,yf-sun21,yl-wang19,lijx19,sunsq21}@mails.tsinghua.edu.cn, {jiangkun, ydg}@mail.tsinghua.edu.cn

Abstract

Detection And Tracking of Moving Objects (DATMO) is an essential component in environmental perception for autonomous driving. While 3D detectors using surround-view cameras are just flourishing, there is a growing tendency of using different transformer-based methods to learn queries in 3D space from 2D feature maps of perspective view. This paper proposes Sparse R-CNN 3D (SRCN3D), a novel two-stage fully-convolutional mapping pipeline for surround-view camera detection and tracking. SRCN3D adopts a cascade structure with twin-track update of both fixed number of proposal boxes and proposal latent features. Proposal boxes are projected to perspective view so as to aggregate Region of Interest (RoI) local features. Based on that, proposal features are refined via a dynamic instance interactive head, which then generates classification and the offsets applied to original bounding boxes. Compared to prior arts, our sparse feature sampling module only utilizes local 2D features for adjustment of each corresponding 3D proposal box, leading to a complete sparse paradigm. The proposal features and appearance features are both taken in data association process in a multi-hypotheses 3D multi-object tracking approach. Extensive experiments on nuScenes dataset demonstrate the effectiveness of our proposed SRCN3D detector and tracker. Code is available at <https://github.com/synsin0/SRCN3D>.

Introduction

Environmental perception is an essential task in the field of autonomous driving. DATMO in environmental perception, is responsible for classifying and localizing the dynamic objects of interest (vehicles, pedestrians, cyclists and others) via the detector, as well as record their unique labels and past trajectories in the tracker.

Cameras are ubiquitous sensors equipped in autonomous vehicles. Compared to high-resolution lidars, cameras take advantage of lower price, higher angular resolution and denser information in the distance. We point out two long-standing challenges existing for camera-only detection methods. As cameras have no geometric or depth cues, 3D reconstruction of real-world scale from 2D images is an ill-conditioned problem. Another issue is cross-view fusion, namely, two adjacent surround-view cameras each see a part of one large-scale object, but the object needs to be detected as a whole. At present,

lidar detectors benefit from geometric cues and are able to generate more accurate detection results, while newly emerging camera-only detectors rise rapidly in accuracy thanks to latest innovation of data-driven feature transformation from perspective view to 3D world space.

Our proposed method, SRCN3D, is a simple and elegant pipeline following the cascade structure and set-prediction approach highly inspired by Sparse R-CNN (SRCN) (Sun et al. 2021). We adopt a commonly used backbone and Feature Pyramid Network (FPN) (Lin et al. 2017a) neck, but a brand-new SRCN3D head which iteratively updates both 3D proposal boxes and proposal features at the same time, so that the final refined proposal boxes are directly detection results without complicated post-processing step or regression process from latent features. Our framework replaces transformer structure with fully-convolutional network, without the need of masking operation or positional embedding of multi-camera multi-level feature maps. It achieves a combination of interaction between proposal feature interaction in multi-head attention among object proposals, and local attention between boxes and RoIs in feature maps.

The core question is how 2D features should be organized to adjust proposal boxes in order to better fit real-world objects. We propose a novel sparse feature sampling module between 2D feature maps and 3D predicted bounding boxes for cross-attention multi-camera multi-level feature organization. Fig. 1 illustrates the comparison of interaction mechanism between three typical realizations of cascade multi-view 3D detectors, namely DETR3D (Wang et al. 2021b), BEVFormer (Li et al. 2022) and SRCN3D. DETR3D (Wang et al. 2021b) finds values of queries on a reference point, and the values are aggregations of grid sample features from projected 2D points on feature maps. It utilizes mainly global attention between queries and all possible values. BEVFormer (Li et al. 2022) poses queries on Bird’s-Eye-View (BEV) grids and exploits spatial local features via deformable attention in a local region of attentive area in feature maps. It reaches a balance between global and local attention, but consumes large memory and suffers from time-consuming training. Our proposed module replaces transformer-style global attention with CNN-style local attention, which uses only local features acquired by RoI operation and simple aggregation for refinement of proposal boxes. Experiments demonstrate our proposed method works with fewer proposals, and is conse-

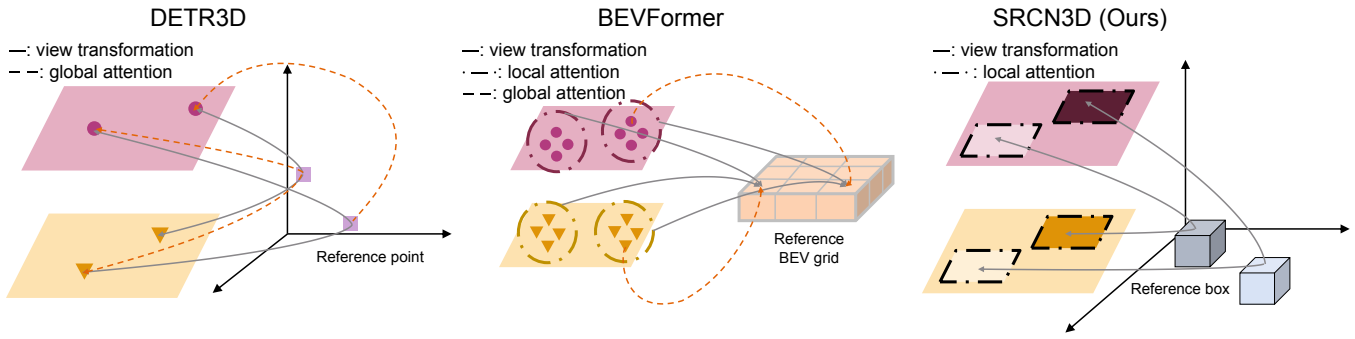


Figure 1: Comparison between typical cascade structure multi-view 3D detectors. Different from transformer-based DETR3D (Wang et al. 2021b) and BEVFormer (Li et al. 2022), SRCN3D uses proposal boxes as intermediate containers and utilizes only local attention for feature transformation and sampling.

quently more efficient in computation.

In summary, the contributions of this paper can be summed up as follows:

- To the best of our knowledge, **the first fully-convolutional two-stage 3D->2D mapping multi-view camera 3D object detection approach**. The pipeline is straightforward, lightweight, slightly faster than DETR3D (Wang et al. 2021b) and BEVFormer (Li et al. 2022).
- **A novel sparse cross-attention module between 3D proposals and 2D feature maps**, which replaces global attention with local dynamic instance interaction head, involving fewer queries, thus leading to lower computation cost.
- **A novel probabilistic feature-embedding multi-object tracking approach**, which takes advantage of hybrid motion features, proposal features and RoI features in data association process.

Related Work

2D Object Detection

A common taxonomy for 2D object detection consists of two-stage detection, one-stage detection and set-prediction detection. R-CNN family (Girshick et al. 2014; Girshick 2015; He et al. 2015) is the pioneer of two-stage 2D object detection. Faster R-CNN (Ren et al. 2015) makes use of Region Proposal Network (RPN) for dense-to-sparse candidate regions. One-stage methods like YOLO (Redmon et al. 2016) and SSD (Carion et al. 2020a), merge two stages into one and further accelerate training and inference, but they need rather larger numbers of proposals and post-processing step like non-maximum suppression (NMS). Set-prediction methods originate from DETR (Carion et al. 2020b), which learn a fixed number of object queries that are comparable to the number of ground truth. Hungarian matching and a bipartite loss are adopted. SRCN (Sun et al. 2021) introduces an inherent sparse paradigm for two-stage learnable RPN candidates. The sparse paradigm provides us with insights of new pipeline for multi-view 3D object detection.

Multi-camera 3D Object Detection

There are three paradigms of state-of-the-art multi-view camera 3D object detectors, which are *2D+BEV*, *2D->3D*

Pseudo Lidar, and *3D->2D mapping*. *2D+BEV* is to predict 3D boxes from perspective view 2D images and perform BEV aggregation (Wang et al. 2021a; Wang et al. 2022; Zhang et al. 2022; Park et al. 2021). The second series performs depth estimation first, then transforms to world coordinate and aggregates pointclouds (Huang et al. 2021; Huang and Huang 2022), addressing the detection problem in a bottom-up fashion. However, the difficulty of depth estimation is prone to subsequent reconstruction errors. The third paradigm proposes 3D queries at the very beginning, then undergoes a cascade refinement structure (Wang et al. 2021b; Liu et al. 2022a; Li et al. 2022). It demonstrates competitive potential thanks to no explicit depth estimation and inherent cross-view fusion mechanism, and often leads to better performance. Our proposed method adopts the *3D->2D mapping* paradigm and designs a novel two-stage pipeline which is different from existing works.

Transformer-based Object Detection

Vision transformer models are gaining growing attention. DETR (Carion et al. 2020b) adopts a set-prediction paradigm, where a set of proposed object queries interact with global image features. Deformable DETR (Zhu et al. 2020) invents deformable attention, where each query and reference point interact with local regions of interest. Furthermore, SRCN (Sun et al. 2021) puts forward a completely sparse schema, where each proposal box interacts only with its specific proposal feature. Transformer-style attention mechanism is also borrowed and realized in 3D object detection, where cross-attention between 3D queries and 2D feature maps is frequently applied (Wang et al. 2021b; Li et al. 2022; Liu et al. 2022a; Liu et al. 2022b). DETR3D (Wang et al. 2021b) is the first to apply a top-down framework, which projects reference points on feature maps and performs cross-attention to refine proposal features. BEVFormer (Li et al. 2022) leverages cross-attention on bird’s eye view (BEV) grid features, performs spatial deformable attention for BEV grids and temporal alignment of BEV features. PETR (Liu et al. 2022a) and PETRv2 (Liu et al. 2022b) adopt idea from implicit neural representation and project 2D features map to 3D space so as to interact with 3D queries. 3D detectors mentioned above utilize transformer’s global attention for feature sampling

from 2D to 3D space, while our method explores a sparse feature sampling module without global attention and makes itself a purely sparse method.

3D Multi-Object Tracking

MOT is another challenging task right after object detection, aiming to temporally associate trajectories of each same object and record its unique label. Data association is the core issue of MOT, where the dominant matching approach is Global Nearest Neighbor (GNN), realized in the form of Hungarian or Greedy algorithm used in AB3DMOT (Weng et al. 2020). Another approach is Random Finite Set (RFS) (García-Fernández et al. 2017), an online multi-hypotheses paradigm circumventing deterministic one-to-one pair matching. Current MOT research, e.g. CenterTrack (Zhou, Koltun, and Krähenbühl 2020) and QD-3DT (Hu et al. 2022), focuses on utilizing implicit features to express matching similarity in the embedded space, empowering the network to identify the same object based on appearance features through re-identification (Re-ID) process. Our MOT tracker explores a novel multi-hypotheses probabilistic mode of data association with hybrid feature embedding.

Sparse R-CNN 3D

Overview

Problem Formulation. 3D object detection for autonomous driving perception system aims to classify the objects of interests into according categories and predict 3D bounding boxes given camera images and corresponding camera parameters. Basically, each 3D bounding box is represented by parameters including its translation $[x, y, z]$, dimension $[w, l, h]$, rotation θ and velocity $[v_x, v_y]$. Multi-object tracking associates detected objects in temporal dimension and records the unique label and past trajectories of each object of interest.

Architecture. The overall framework of SRCN3D is illustrated in Fig. 2. SRCN3D has a novel two-stage fully-convolutional 3D object detection architecture. We build our architecture based on the following consideration:

- We estimate 3D bounding boxes directly in 3D world space, while 2D images in perspective view serve as implicit cues in our network. Transformation from 3D proposals to 2D images follows a standard camera model.
- Following a sparse paradigm, we apply a cascade structure to refine both proposal boxes and features. Proposal boxes serve as filters to focus on interested local regions of 2D feature maps. Proposal features classify the objects and provide adjustment cues of proposal boxes.
- We design a fully-convolutional pipeline in contrast to vision transformer-based detectors, so we don't need mask operations and positional embeddings on feature maps. We only extract local feature with RoIAlign, getting rid of global attention weights in feature sampling between 3D proposals and 2D features maps.
- We avoid explicit depth estimation and depth supervision, as well as 3D reconstruction of pseudo pointclouds and post-processing step like NMS.

The architecture of SRCN3D consists of three important modules, a backbone, a standard FPN (Lin et al. 2017a) neck, and a novel SRCN3D head. First of all, we feed the RGB images into a backbone network (e.g. ResNet-101 (He et al. 2016)) with FPN (Lin et al. 2017a) architecture to generate multi-level feature maps $\{F_1^i, F_2^i, F_3^i, F_4^i\}_{i=1}^{N_{cam}}$ for each view. As the beginning of SRCN3D head, we start from a fixed set of 3D learnable proposal boxes and proposal features, and the initial parameters for boxes and features are randomly initialized and learnable during training process. In a cascade structure, the proposal boxes and proposal features have a strict one-to-one correspondence, and they are updated in a twin-track approach towards classification and localization of objects. Proposal boxes are updated in a box adjustment step and proposal features are updated with a sparse feature sampling module.

SRCN3D Head

As shown in Fig. 3, SRCN3D head composes of three key modules, a sparse feature sampling module for feature extraction, a Dynamic Instance Interactive module (DII head) for feature refinement and an adjustment module for box refinement. For each round of iteration there are two inputs, a fixed set of learnable proposal boxes and proposal features. SRCN3D head refines the predicted boxes through cascade structure and then outputs final detection which is close to the surrounding objects of the real world. Each round of bounding box forward process includes the following steps:

- Restore proposal boxes to world scale, get eight corner points and project corner points to images using different intrinsic and extrinsic camera parameters.
- Collect four borderline corner points on each images to form a ROI candidate, sample ROI features using RoIAlign and aggregate cross-view ROI features as input of DII head.
- Undergo 3D DII head for refinement of object features and output cues for box adjustment.
- Refine location, dimension, rotation and velocity with box adjustment module, operate normalization on 3D position of boxes and prepare the input for the next round.

DII head benefits from light convolutional design and shows great performance with lower computation cost in 2D object detection (Sun et al. 2021). In detail, two 1×1 convolutional layers are designed in DII head for interaction, followed by a Feed-Forward Network (FFN) block with layer normalization to generate new object features and a linear projection block to output classification and regression predictions. Local interaction mechanism is implemented by applying 1×1 convolutional kernels on ROI features extracted from proposal boxes and generating corresponding parameters based on proposal features through linear transformation.

3D proposal boxes are defined as a fixed number of boxes parameterized to the same dimension as 3D bounding box (e.g. $\{B_i\}_{i=1}^N \subset R^{10}, N = 300$). The 10 dimensions are defined as $[c_x, c_y, h, w, c_z, l, \cos\theta, \sin\theta, v_x, v_y]$, where c_x, c_y, c_z are center coordinates of the box, h, w, l are height,

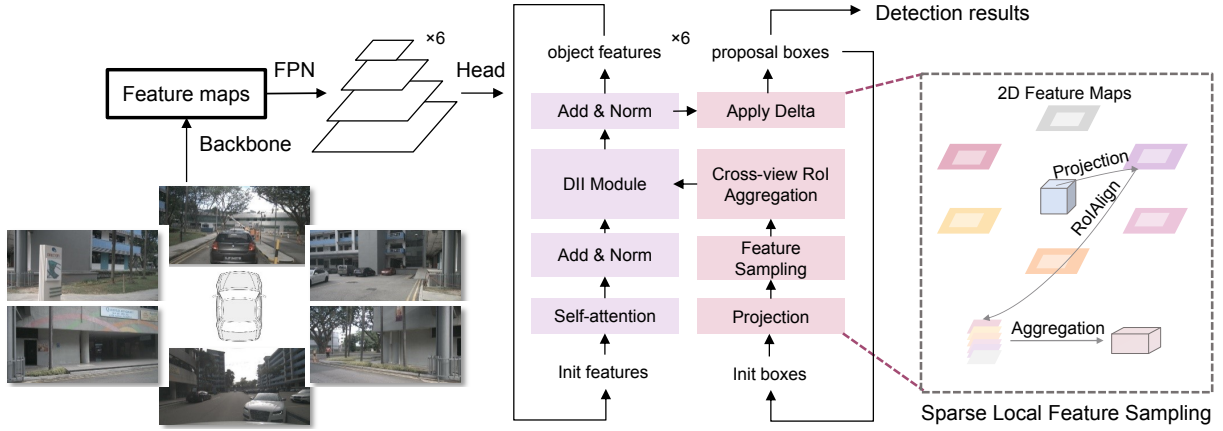


Figure 2: The framework of SRCN3D. Taken camera images as inputs, SRCN3D contains a backbone network with FPN enhancement to extract 2D feature maps and a twin-track detection module. Meanwhile, a sparse feature sampling module is designed to extract RoIs.

weight and length, θ is the yaw angle and v_x, v_y are velocities.

Proposal features are represented by sets of high-dimensional latent vectors (e.g. $\{f_i\}_{i=1}^N \subset R^{256}$), corresponding to proposal boxes one by one. We also apply a self-attention module to proposal features as SRCN (Sun et al. 2021) does before DII head.

Sparse Feature Sampling Module. Learnable 3D proposal boxes are utilized as sparse candidates and updated iteratively. To facilitate the use of 3D information, we decode 3D proposal boxes from center points to box corners through simple geometric transformation. For simplicity, we refer i th decoded box as a set of 3-d dimensional vectors $\{C_{il}\}_{l=1}^8 \subset R^3$ denoting the coordinates of corner points. Motivated by DETR3D (Wang et al. 2021b), these proposal boxes are projected into each one of feature maps using the camera transformation matrices as follows:

$$C_{il}^* = C_{il} \oplus 1, C_{mil} = T_m C_{il}^*, \quad (1)$$

where $l = 1, \dots, 8, m = 1, \dots, N_{cam}, C_{mil} = (C_{milx}, C_{mily}, 1)$ and T_m denotes the camera transformation matrix. Then the projected boxes on each camera can be easily obtained as follows:

$$\tilde{B}_{im} = (\min_l C_{mlx}, \min_l C_{mly}, \max_l C_{mlx}, \max_l C_{mly}), \quad (2)$$

where $i = 1, \dots, N, m = 1, \dots, N_{cam}$.

As shown in Fig. 3, given the projected boxes, we use RoIAlign operation to extract features of interest. The projection of box corner points may result in three cases. The normal case indicates a projected 2D box on images. If the projected points have a negative depth, the box locates behind the camera, which is naturally invisible. If the projected corners are outside or partially outside the pixel space, the box is (partially) invisible. The latter two abnormal feature sampling cases result in empty or partially empty RoI features via RoIAlign, so that masking operations and positional encoding techniques are deftly avoided.

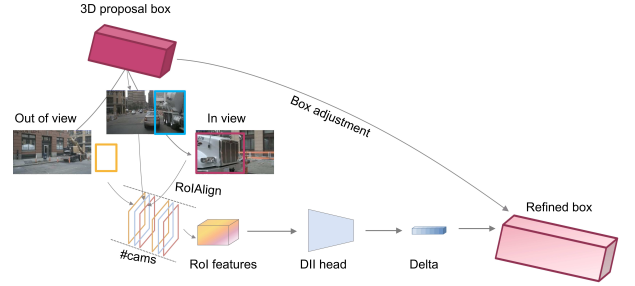


Figure 3: A graphical illustration of sparse feature sampling module. In the sparse feature sampling module, 3D proposal boxes are initialized and projected into feature maps in the camera plane for RoI extraction. After aggregation, RoI features interact with proposal features in DII head which outputs results for refinement. Finally, box adjustment module enhances the box predictions.

Cross-view fusion. Before entering the prediction head, corresponding RoI features on multi-view camera images are aggregated to guarantee cross-view fusion learning. In this way, no matter how many cameras capture one proposal box, the RoI features maintain a fixed expression structure.

Box Adjustment

Here we define the predicted boxes and cues (fine-tuning values) in t th stage as $\{b_i^t\}_{i=1}^N$ and $\{\Delta b_i^t\}_{i=1}^N$ respectively. Then the box adjustment operation for location and dimension parameters can be formulated as follows:

$$\begin{cases} b_{ix}^{t+1} = \Delta b_{ix}^{t+1} \times b_{iw}^t + b_{ix}^t \\ b_{iy}^{t+1} = \Delta b_{iy}^{t+1} \times b_{il}^t + b_{iy}^t \\ b_{iz}^{t+1} = \Delta b_{iz}^{t+1} \times b_{ih}^t + b_{iz}^t \end{cases} \quad (3)$$

Considering non-negative constraints, dimension parameters are usually in the form of logarithm. Therefore, its adjustment

is formulated as follows:

$$\begin{cases} b_{iw}^{t+1} = e^{\Delta b_{iw}^{t+1}} \times b_{iw}^t \\ b_{il}^{t+1} = e^{\Delta b_{il}^{t+1}} \times b_{il}^t \\ b_{ih}^{t+1} = e^{\Delta b_{ih}^{t+1}} \times b_{ih}^t \end{cases} . \quad (4)$$

As for rotation and velocity, we directly take the values in $\{\Delta b_i^t\}_{i=1}^N$ as the predicted results of t th stage.

Loss Design

Generally, the loss function of SRCN3D is a linear combination of a Focal Loss (Lin et al. 2017b) for category classification and a L1 norm loss for 3D bounding box regression, which is as follows:

$$\mathcal{L} = \omega_{cls} \times \mathcal{L}_{cls} + \omega_{l_{reg}} \times \mathcal{L}_1. \quad (5)$$

SRCN3D employs set-prediction loss following DETR (Carion et al. 2020b). In a set-to-set prediction, the loss function is optimized based on an optimal bipartite matching between the predictions and ground truth sets. Hungarian algorithm is implemented to produce the optimal assignment. Assuming there are N predictions denoted by $\{(\hat{c}_i, \hat{b}_i)\}_{i=1}^N$, the ground truth set $\{(c_i, b_i)\}_{i=1}^N$ is padded to the same size with \emptyset . Then the matching cost can be written as $\sum_{i=1}^N [-\log \hat{p}_{\sigma^*(i)}(c_i) + \mathbb{I}_{\{c_i \neq \emptyset\}} \mathcal{L}_1(b_i, \hat{b}_{\sigma^*(i)})]$, where

$\sigma^* = \arg \min_{\sigma} \sum_{i=1}^N [\hat{p}_{\sigma(i)}(c_i) + \mathbb{I}_{\{c_i \neq \emptyset\}} \mathcal{L}_1(b_i, \hat{b}_{\sigma(i)})]$ denotes the optimal index ranking.

Multi-object Tracking and Re-identification

Multi-object Tracking mainly handles data association of detected objects between past and current frames. Given the fact that camera-only detectors don't provide detection results as high-quality as lidar detectors, we adopt a hypothesis-oriented probabilistic approach, Multi-Bernoulli Mixture (MBM) to deal with uncertain data association. MBM treats data association into global hypotheses and single target hypotheses. The MBM density is defined as sum of j global hypotheses as follows:

$$f^{\text{mbm}}(X) \propto \sum_j \sum_{X_1 \uplus \dots \uplus X_n = X} \prod_{i=1}^n w_{j,i} f_{j,i}(X_i), \quad (6)$$

where $f^{\text{mbm}}(X)$ is the posterior of MBM intensity, X is the whole set of detected objects, $w_{j,i}$ indicates the weight of a Bernoulli component X_i in global hypothesis j , and $f_{j,i}(X_i)$ is the probability intensity of single Bernoulli component X_i in global hypothesis j defined as follows:

$$f_{j,i}(X_i) = \begin{cases} 1 - r_{j,i} & \text{if } X_i = \emptyset \\ r_{j,i} p_{j,i}(x) & \text{if } X_i = x \\ 0 & \text{otherwise} \end{cases}, \quad (7)$$

where $r_{j,i}$ denotes the existence probability of object x in single target hypothesis (STH) X . $p_{j,i}$ is the probability density function considering the log likelihood of the hypothesis target. Each STH denotes one object detected or a missed

detection. Temporal prediction and update of states follow a standard unscented kalman filter. One indispensable operation for any data association is to compute likelihood or similarity between measurements and states. In SRCN3D tracker, each measurement includes motion features and the properties of the 3D bounding box, namely RoI features and proposal features. The likelihood of 3D bounding boxes is computed by mahalanobis distance introduced in (Chiu et al. 2021), and latent RoIs and proposal features follow a cosine similarity between feature vectors. The overall likelihood is set as

$$l = l_{motion} + \alpha \times l_{RoI} + \beta \times l_{prop}. \quad (8)$$

In practice, we set $\alpha = \beta = 0.5$ to achieve a balance among various measurements and states.

Experiments

Dataset

We present experiment results on the nuScenes dataset (Caesar et al. 2020), which includes 1000 driving scenes of about 20 seconds duration. Each key frame is annotated at 2Hz. RGB image samples are collected from 6 cameras with known intrinsic and extrinsic camera parameters. In our experiment, the dataset contains about 40k annotated samples and splits 70%, 15%, 15% samples for training, validation and testing, respectively. All samples are classified into 10 categories according to nuScenes detection challenge.

Metrics

We adopt the nuScenes (Caesar et al. 2020) official evaluation protocol. As for detection metrics, we adopt true positive metrics (TP metrics) including average translation error (ATE), average scale error (ASE), average orientation error (AOE), average velocity error (AVE), and average attribute error (AAE). Besides, we measure mean average precision (mAP) and nuScenes Detection Score (NDS) to compare our performance with state-of-the-art (SOTA) detectors. Tracking metrics are based on CLEARMOT (Bernardin and Stiefelhaagen 2008), mainly including average multi object tracking accuracy (AMOTA) and average multi object tracking precision (AMOTP).

Training and Inference

Pipeline. We only use RGB images from 6 cameras for input modality without external training data. The bounding box of each detected object is predicted in ego vehicle coordinate and transformed into world coordinate for multi-object tracking and evaluation. The score thresholds for detection and tracking are both 0.2.

Training. Our code is built upon the MMDetection3D (MMDetection3D Contributors 2020) infrastructure. To efficiently extract 2D features, we employ ResNet101 (He et al. 2016) pretrained on FCOS3D (Wang et al. 2021a) and PGD (Wang et al. 2022) as the backbone network. The first stage of backbone is frozen and the last two stages are with Deformable Convolutional Networks (Zhu et al. 2019b) (DCNv2). We use a hybrid bipartite loss via 3D Hungarian assigner, which consists of a Focal Loss (Lin et al. 2017b) with weight 2.0 and a L1 loss with weight 0.25. The model

Table 1: Comparison of SOTA detectors on nuScenes detection val set. ‡: with test-time augmentation. §: trained with CBGS (Zhu et al. 2019a). ¶: initialized from pretrained FCOS3D (Wang et al. 2021a) backbone.

Method	Size	Backbone	NDS↑	mAP↑	mATE↓	mASE↓	mAOE↓	mAVE↓	mAAE↓
CenterNet (Duan et al. 2019)	-	DLA	0.328	0.306	0.716	0.264	0.609	1.426	0.658
FCOS3D ‡(Wang et al. 2021a)	1600×900	Res-101	0.415	0.343	0.725	0.263	0.422	1.292	0.153
DETR3D ¶(Wang et al. 2021b)	1600×900	Res-101	0.425	0.346	0.773	0.268	0.383	0.842	0.216
BEVDet §(Huang et al. 2021)	1056×384	Swin-T	0.403	0.322	0.664	0.266	0.508	0.894	0.243
BEVFormer-S ¶(Li et al. 2022)	1600×900	Res-101	0.448	0.375	0.725	0.272	0.391	0.802	0.200
PETR §(Liu et al. 2022a)	1408×512	Res-101	0.421	0.357	0.710	0.270	0.490	0.885	0.224
SRCN3D (Ours)¶	1600×900	Res-101	0.428	0.337	0.779	0.287	0.367	0.781	0.188

Table 2: Comparison of SOTA detectors on nuScenes detection test set. Detection methods using temporal aggregation are not included. †: trained using extra data. ‡: with test time augmentation.

Method	Backbone	NDS↑	mAP↑	mATE↓	mASE↓	mAOE↓	mAVE↓	mAAE↓
CenterNet (Duan et al. 2019)	DLA	0.400	0.338	0.658	0.255	0.629	1.629	0.142
FCOS3D ‡(Wang et al. 2021a)	Res-101	0.428	0.358	0.690	0.249	0.452	1.434	0.124
DETR3D †(Wang et al. 2021b)	V2-99	0.479	0.412	0.641	0.255	0.394	0.845	0.133
DD3D †‡(Park et al. 2021)	V2-99	0.477	0.418	0.572	0.249	0.368	1.014	0.124
BEVDet †(Huang et al. 2021)	V2-99	0.482	0.422	0.529	0.236	0.395	0.979	0.152
PGD ‡(Wang et al. 2022)	Res-101	0.448	0.386	0.626	0.245	0.451	1.509	0.127
PETR †(Liu et al. 2022a)	V2-99	0.504	0.441	0.593	0.249	0.383	0.808	0.132
BEVFormer-S (Li et al. 2022)	Res-101	0.462	0.409	0.650	0.261	0.439	0.925	0.147
SRCN3D (Ours)	Res-101	0.412	0.347	0.723	0.278	0.472	0.986	0.158

is trained using AdamW optimizer with weight decay of 0.01. The learning rate is initialized with $2e^{-4}$ and decays with cosine annealing policy. We set the detection region to $[-61.2m, 61.2m]$ for the X and Y axis, and $[-5m, 3m]$ for the Z axis. All experiments are trained for 24 epochs on 2 RTX3090 GPUs.

Inference. In the inference process, SRCN3D makes simple predictions without any post-processing step such as NMS and test-time augmentation (TTA). Consequently, our model infers within 2.9 FPS on a single RTX3090 GPU, faster than other cascade-structure multi-view detectors like DETR3D (2.7 FPS) and BEVFormer (2.1 FPS).

Comparison with SOTA methods

As shown in Table. 1, we compare the performance with SOTA methods on nuScenes validation set. It shows that SRCN3D achieves competitive performance on both NDS and mAP metrics. In comparison to typical monocular 3D object detection methods CenterNet (Duan et al. 2019) and FCOS3D (Wang et al. 2021a), SRCN3D with ResNet-101 (He et al. 2016) backbone surpasses them on NDS by 10.0% and 1.3%, respectively. Besides, we also compare SRCN3D with multi-view 3D object detection methods DETR3D (Wang et al. 2021b), BEVDet (Huang et al. 2021) and PETR (Liu et al. 2022a). Our method outperforms them 0.3%, 2.5% and 0.7% in NDS, respectively. As for TP metrics, SRCN3D achieves the best performance on mAOE and mAVE.

Table 2 shows the performance comparison on nuScenes test set. Our method achieves competitive performance on NDS, mAP and other true positive metrics. All the experimental results demonstrate the effectiveness of our method on 3D object detection task.

We also present the comparison with state-of-the-art methods on nuScenes tracking benchmark. Compared with latest methods like QD-3DT (Hu et al. 2022) and PolarDETR (Chen et al. 2022), our method achieves the best performance on ATOMA and competitive performance on AMOTP, which indicates the excellence of SRCN3D on tracking tasks.

Ablation Study

Ablation on key modules. Key components for SRCN3D are learnable boxes, DII module, and box adjustment step. The ablation is implemented by replacing these modules in SRCN3D with similar parts in DETR3D (Wang et al. 2021b). When learnable boxes are removed, a quasi single-stage cross attention module is applied where boxes are regressed directly by a regression branch of proposal features at the beginning. Model without DII head uses a standard attention weight to get global attention between proposals and apply average pooling of RoI features. Model without box adjustment step produces boxes estimation by directly inputting object features after DII head into regression branch. The above three cases are trained and evaluated independently.

Table 3: Ablation on key modules. Modules are replaced from a standard realization of SRCN3D.

Modules	NDS	mAP
w/o learnable box	0.310	0.249
w/o DII head	0.331	0.248
w/o box adjustment	0.307	0.229
All	0.428	0.337

Table 5: Comparison of SOTA trackers on nuScenes tracking benchmark. Quantitative results are from original paper or nuScenes leaderboard.

Method	Modality	Split	ATOMA \uparrow	AMOTP \downarrow
QD3DT (Hu et al. 2022)	Camera	test	0.217	1.550
Megvii-AB3DMOT (Weng et al. 2020)	Lidar	test	0.151	1.501
CenterTrack-Open (Zhou, Koltun, and Krähenbühl 2020)	Lidar + Camera	test	0.108	0.989
PolarDETR (Chen et al. 2022)	Camera	test	0.273	1.185
DEFT (Chaabane et al. 2021)	Camera	test	0.177	1.564
SRCN3D (Ours)	Camera	val	0.333	1.426

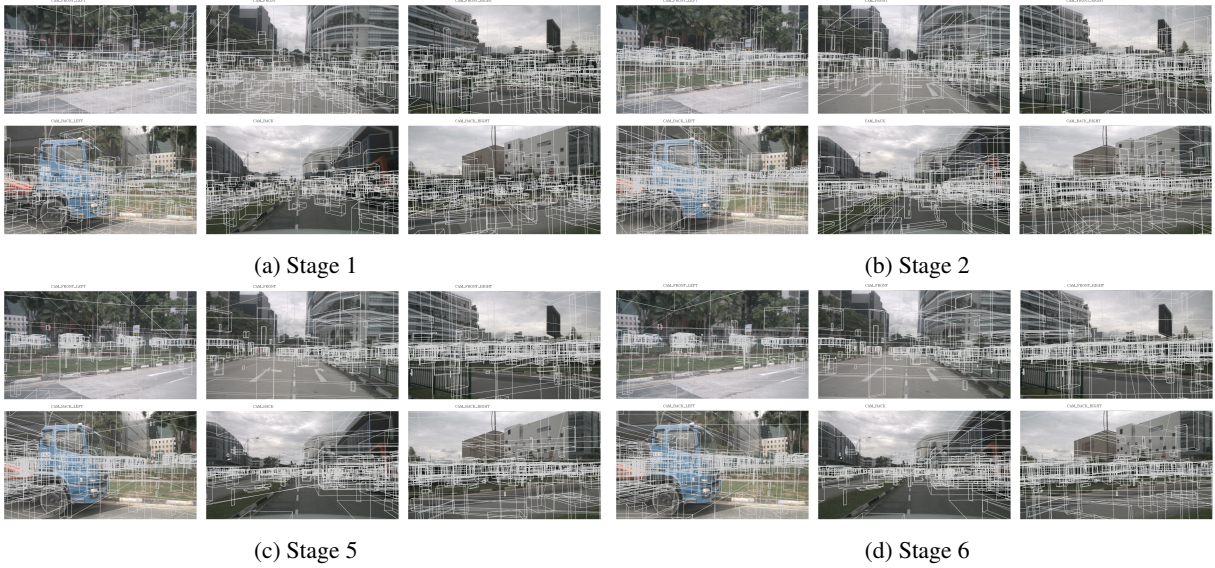


Figure 4: Visualization of learnable proposal boxes of some stages on nuScenes val set. As the stage increases, boxes in images locate more densely on area of objects. That is, proposal boxes show a complete coverage of possible location of detected objects.

Table. 3 shows that three key modules are rather indispensable in the whole pipeline of SRCN3D. Replacing any single one with transformer-type counterparts greatly reduces the final performance.

Table 4: Ablation on the number of proposal boxes and features.

Number of proposals	NDS	mAP
900	0.428	0.337
300	0.413	0.322

Number of proposals. The number of proposal box and feature is related to GPU memory and inference speed. Table. 4 indicates that when we reduce the number of proposals to a rather low amount, the quantitative results show slight decrease compared to the heavy version. It demonstrates that our sparse feature sampling module is capable to capture region of interests with only local features.

Visualization

In this section, we mainly provide visualization results on the validation set with ground truth annotations. Fig.5 visualizes final detection results in the camera front view and bird’s-eye view. Overall, as shown in the bird’s-eye view, the predicted boxes are close to the ground truth ones. In the camera canvas, it can be observed that small movable objects (e.g. traffic cones) and partially blocked objects (e.g. the vehicle in the back-left camera view) are also detected precisely. These results indicate a good detection performance of SRCN3D.

Cross-view fusion. The effect of cross-view fusion is that objects appearing in multiple perspectives can be detected as a whole through boxes partially inside the views. As shown in Fig.6, the same object that appears in two perspectives is framed as one. This demonstrates that the ROI aggregation strategy in sparse feature sampling module successfully realizes cross-view fusion detection.

Sparse Local Attention. Fig.4 visualizes all 3D proposal boxes of each stages in camera front views. The iterations of proposal boxes show a tendency from arbitrary distribution on the whole images to target areas and appropriate sizes. This process shows that SRCN3D head can capture semantic

characteristics well with small sets of regional proposals and local attention mechanism, so that convergence is guaranteed during the cascade refinement.

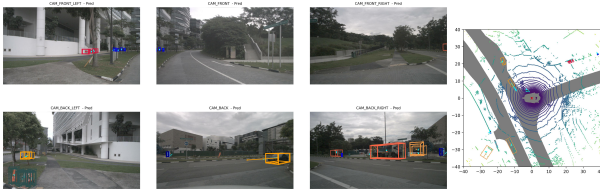


Figure 5: Visualization of final predictions and ground truth boxes on nuScenes val set. Ground truth boxes are drawn with green arrows and the others are predicted results. Different colors of box frames refer to true annotations for ground truth samples and predicted classes for predicted boxes. For example, the dark green, orange, red and blue boxes corresponds to traffic cones, vehicles, bicycles and pedestrians, respectively.



Figure 6: Visualization of a successful example of cross-view fusion. Both in the left-front and front camera view, the white car appears, which is framed as a whole object by two boxes partially shown in each perspective.

Conclusion

This paper proposes a novel innovative architecture, SRCN3D, which can efficiently extract and fuse cross-view features, detect and track objects of interest. Our insight is that box-feature twin-track proposals and cascade-style refinement process with only local RoI attention enable 3D object detection and cross-view fusion. We hope that this architecture can serve as a foundation for fully-sparse surround-view 3D object detection. In the future, the authors will investigate deeper in combining 2D segmentation and temporal information to enhance the accuracy and robustness of the detector.

Acknowledgments

This work was supported by National Natural Science Foundation of China (U1864203) and in part by National Natural Science Foundation of China (61903220).

References

[Bernardin and Stiefel-hagen 2008] Bernardin, K., and Stiefel-hagen, R. 2008. Evaluating multiple object tracking performance: The clear mot metrics. *J. Image Video Process.* 2008.

[Caesar et al. 2020] Caesar, H.; Bankiti, V.; Lang, A. H.; Vora, S.; Liong, V. E.; Xu, Q.; Krishnan, A.; Pan, Y.; Baldan, G.; and Beijbom, O. 2020. nuscenes: A multimodal dataset for autonomous driving. In *Proceedings of the IEEE/CVF conference on computer vision and pattern recognition*, 11621–11631.

[Carion et al. 2020a] Carion, N.; Massa, F.; Synnaeve, G.; Usunier, N.; Kirillov, A.; and Zagoruyko, S. 2020a. End-to-end object detection with transformers. In *European conference on computer vision*, 213–229. Springer.

[Carion et al. 2020b] Carion, N.; Massa, F.; Synnaeve, G.; Usunier, N.; Kirillov, A.; and Zagoruyko, S. 2020b. End-to-end object detection with transformers. In *European conference on computer vision*, 213–229. Springer.

[Chaabane et al. 2021] Chaabane, M.; Zhang, P.; Beveridge, J. R.; and O’Hara, S. 2021. Deft: Detection embeddings for tracking. *arXiv preprint arXiv:2102.02267*.

[Chen et al. 2022] Chen, S.; ; Wang, X.; Cheng, T.; Zhang, Q.; Huang, C.; and Liu, W. 2022. Polar parametrization for vision-based surround-view 3d detection. *arXiv:2206.10965*.

[Chiu et al. 2021] Chiu, H.-K.; Li, J.; Ambruş, R.; and Bohg, J. 2021. Probabilistic 3d multi-modal, multi-object tracking for autonomous driving. In *2021 IEEE International Conference on Robotics and Automation (ICRA)*, 14227–14233.

[Duan et al. 2019] Duan, K.; Bai, S.; Xie, L.; Qi, H.; Huang, Q.; and Tian, Q. 2019. Centernet: Keypoint triplets for object detection. In *Proceedings of the IEEE/CVF international conference on computer vision*, 6569–6578.

[García-Fernández et al. 2017] García-Fernández, A.; Williams, J.; Granström, K.; and Svensson, L. 2017. Poisson multi-bernoulli mixture filter: direct derivation and implementation. *IEEE Transactions on Aerospace and Electronic Systems* PP.

[Girshick et al. 2014] Girshick, R.; Donahue, J.; Darrell, T.; and Malik, J. 2014. Rich feature hierarchies for accurate object detection and semantic segmentation. In *Proceedings of the IEEE conference on computer vision and pattern recognition*, 580–587.

[Girshick 2015] Girshick, R. 2015. Fast r-cnn. In *Proceedings of the IEEE international conference on computer vision*, 1440–1448.

[He et al. 2015] He, K.; Zhang, X.; Ren, S.; and Sun, J. 2015. Spatial pyramid pooling in deep convolutional networks for visual recognition. *IEEE transactions on pattern analysis and machine intelligence* 37(9):1904–1916.

[He et al. 2016] He, K.; Zhang, X.; Ren, S.; and Sun, J. 2016. Deep residual learning for image recognition. In *Proceedings of the IEEE conference on computer vision and pattern recognition*, 770–778.

[Hu et al. 2022] Hu, H.-N.; Yang, Y.-H.; Fischer, T.; Darrell, T.; Yu, F.; and Sun, M. 2022. Monocular quasi-dense 3d object tracking. *IEEE Transactions on Pattern Analysis and Machine Intelligence*.

[Huang and Huang 2022] Huang, J., and Huang, G. 2022. Bevdet4d: Exploit temporal cues in multi-camera 3d object detection. *arXiv preprint arXiv:2203.17054*.

- [Huang et al. 2021] Huang, J.; Huang, G.; Zhu, Z.; and Du, D. 2021. Bevdet: High-performance multi-camera 3d object detection in bird-eye-view. *arXiv preprint arXiv:2112.11790*.
- [Li et al. 2022] Li, Z.; Wang, W.; Li, H.; Xie, E.; Sima, C.; Lu, T.; Yu, Q.; and Dai, J. 2022. Bevformer: Learning bird’s-eye-view representation from multi-camera images via spatiotemporal transformers. *arXiv preprint arXiv:2203.17270*.
- [Lin et al. 2017a] Lin, T.-Y.; Dollár, P.; Girshick, R.; He, K.; Hariharan, B.; and Belongie, S. 2017a. Feature pyramid networks for object detection. In *Proceedings of the IEEE conference on computer vision and pattern recognition*, 2117–2125.
- [Lin et al. 2017b] Lin, T.-Y.; Goyal, P.; Girshick, R.; He, K.; and Dollár, P. 2017b. Focal loss for dense object detection. In *Proceedings of the IEEE international conference on computer vision*, 2980–2988.
- [Liu et al. 2022a] Liu, Y.; Wang, T.; Zhang, X.; and Sun, J. 2022a. Petr: Position embedding transformation for multi-view 3d object detection. *arXiv preprint arXiv:2203.05625*.
- [Liu et al. 2022b] Liu, Y.; Yan, J.; Jia, F.; Li, S.; Gao, Q.; Wang, T.; Zhang, X.; and Sun, J. 2022b. PetrV2: A unified framework for 3d perception from multi-camera images. *arXiv preprint arXiv:2206.01256*.
- [MMDetection3D Contributors 2020] MMDetection3D Contributors. 2020. MMDetection3D: OpenMMLab next-generation platform for general 3D object detection. <https://github.com/open-mmlab/mmdetection3d>.
- [Park et al. 2021] Park, D.; Amrus, R.; Guizilini, V.; Li, J.; and Gaidon, A. 2021. Is pseudo-lidar needed for monocular 3d object detection? In *Proceedings of the IEEE/CVF International Conference on Computer Vision*, 3142–3152.
- [Redmon et al. 2016] Redmon, J.; Divvala, S.; Girshick, R.; and Farhadi, A. 2016. You only look once: Unified, real-time object detection. In *Proceedings of the IEEE conference on computer vision and pattern recognition*, 779–788.
- [Ren et al. 2015] Ren, S.; He, K.; Girshick, R.; and Sun, J. 2015. Faster r-cnn: Towards real-time object detection with region proposal networks. *Advances in neural information processing systems* 28.
- [Sun et al. 2021] Sun, P.; Zhang, R.; Jiang, Y.; Kong, T.; Xu, C.; Zhan, W.; Tomizuka, M.; Li, L.; Yuan, Z.; Wang, C.; et al. 2021. Sparse r-cnn: End-to-end object detection with learnable proposals. In *Proceedings of the IEEE/CVF conference on computer vision and pattern recognition*, 14454–14463.
- [Wang et al. 2021a] Wang, T.; Zhu, X.; Pang, J.; and Lin, D. 2021a. Fcos3d: Fully convolutional one-stage monocular 3d object detection. In *Proceedings of the IEEE/CVF International Conference on Computer Vision*, 913–922.
- [Wang et al. 2021b] Wang, Y.; Guizilini, V. C.; Zhang, T.; Wang, Y.; Zhao, H.; and Solomon, J. 2021b. DETR3d: 3d object detection from multi-view images via 3d-to-2d queries. In *5th Annual Conference on Robot Learning*.
- [Wang et al. 2022] Wang, T.; Xinge, Z.; Pang, J.; and Lin, D. 2022. Probabilistic and geometric depth: Detecting objects in perspective. In *Conference on Robot Learning*, 1475–1485. PMLR.
- [Weng et al. 2020] Weng, X.; Wang, J.; Held, D.; and Kitani, K. 2020. Ab3dmot: A baseline for 3d multi-object tracking and new evaluation metrics. *arXiv preprint arXiv:2008.08063*.
- [Zhang et al. 2022] Zhang, R.; Qiu, H.; Wang, T.; Xu, X.; Guo, Z.; Qiao, Y.; Gao, P.; and Li, H. 2022. Monodetr: Depth-aware transformer for monocular 3d object detection. *arXiv preprint arXiv:2203.13310*.
- [Zhou, Koltun, and Krähenbühl 2020] Zhou, X.; Koltun, V.; and Krähenbühl, P. 2020. Tracking objects as points. In *European Conference on Computer Vision*, 474–490. Springer.
- [Zhu et al. 2019a] Zhu, B.; Jiang, Z.; Zhou, X.; Li, Z.; and Yu, G. 2019a. Class-balanced grouping and sampling for point cloud 3d object detection. *arXiv preprint arXiv:1908.09492*.
- [Zhu et al. 2019b] Zhu, X.; Hu, H.; Lin, S.; and Dai, J. 2019b. Deformable convnets v2: More deformable, better results. In *Proceedings of the IEEE/CVF conference on computer vision and pattern recognition*, 9308–9316.
- [Zhu et al. 2020] Zhu, X.; Su, W.; Lu, L.; Li, B.; Wang, X.; and Dai, J. 2020. Deformable detr: Deformable transformers for end-to-end object detection. *arXiv preprint arXiv:2010.04159*.